Journal of Colloid and Interface Science 350 (2010) 168–177

Contents lists available at ScienceDirect

Journal of Colloid and Interface Science

www.elsevier.com/locate/jcis

Resonance elastic light scattering (RELS) spectroscopy of fast non-Langmuirian ligand-exchange in glutathione-induced gold nanoparticle assembly

Magdalena Stobiecka, Kaitlin Coopersmith, Maria Hepel *

Department of Chemistry, State University of New York at Potsdam, Potsdam, NY 13676, USA

ARTICLE INFO

Article history:
Received 23 April 2010
Accepted 8 June 2010
Available online 12 June 2010

Keywords:
Glutathione
Gold nanoparticles
Ligand-exchange
Resonance elastic light scattering spectroscopy
Surface plasmon

ABSTRACT

The interactions of a biomolecule glutathione (GSH) with citrate-capped gold nanoparticles (AuNP) have been investigated to evaluate the viability of a rapid GSH-capture by gold nanoparticle carriers, as a model system for applications ranging from designing nanoparticle-enhanced functional biosensor interfaces to nanomedicine. The measurements, performed using resonance elastic light scattering (RELS) spectroscopy, have shown a strong dependence of GSH-induced scattering cross-section on gold nanoparticle size. A large increase in RELS intensity after injection of GSH, in a short reaction time (τ = 60 s), has been observed for small AuNP (5 nm dia.) and ascribed to the fast ligand-exchange followed by AuNP assembly. The unexpected non-Langmuirian concentration dependence of scattering intensity for $AuNP_{5nm}$ indicates on a 2D nucleation and growth mechanism of the ligand-exchange process. The ligand-exchange and small nanoparticle ensemble formation followed by relaxation have been observed in long term (10 h) monitoring of GSH–AuNP interactions by RELS. The results of molecular dynamics and quantum mechanical calculations corroborate the mechanism of the formation of hydrogen-bonded GSH-linkages and interparticle interactions and show that the assembly is driven by multiple H-bonding between GSH-capped AuNP and electrostatic zwitterionic interactions. The RELS spectroscopy has been found as a very sensitive tool for studying interparticle interactions. The application of RELS can be expanded to monitor reactivities and assembly of other monolayer-protected metal clusters, especially in very fast processes which cannot be followed by other techniques.

1. Introduction

The gold nanoparticles (AuNP) have recently gained outstanding interests owing to their size and shape dependent plasmonic optical properties [1–6], ease of functionalization [7–12], and the ability to penetrate the cell membranes. Numerous prospective applications of AuNP relate to the detection of biomolecules [13–16], including DNA strands [17–25], the design of photonic and bioelectronic devices, and the nanomedicine [26–29]. In the latter field, AuNP benefit medical diagnostics, cancer therapy, and contribute to imaging enhancements. The potential application of AuNP in cancer treatment involves targeted drug delivery and photodynamic therapy (PDT). The nanoparticles concentrated in a tumor tissue can deliver chemotherapeutic agents to kill the cancer cells or act as the light scatterers for PDT. In both cases, the specific reactivities of AuNP with biomolecules have to be taken into account. Since the propensity of AuNP to strongly interact with thiol species is one of the most pronounced properties of AuNP, the potential interactions of AuNP with the natural body thiols such as the glutathione (GSH), cysteine (Cys), and homocysteine (Hcys), are of the utmost importance. Therefore, studies of the interactions of functionalized AuNP with GSH and other biomolecules are important not only to elucidate mechanistic issues and describe new phenomena encountered in these systems but also to further the understanding of effects occurring in real tissue environment and to improve the practical therapeutic outcomes.

Glutathione, which adsorbs readily on gold surfaces [10,11,30–32] is a tripeptide (glutamate–cysteine–glycine) with sulfhydryl group able to form a strong Au–S bond. Different kinds of interparticle interactions between GSH, cysteine and homocysteine have been recently discussed by Maye et al. [33]. Such molecules as homocysteine [34,35], glutathione (GSH) [35–37], and aminoacids [35,38–40] have been found to influence the spectral surface-plasmon (SP) characteristics. Previously, we have investigated the interactions and electrochemical reactivity of Hg(II) on GSH-modified gold piezoelectrodes [10,11,41]. The GSH-SAM permeability to ionic species has been demonstrated for Hg(II) [10,11], Pb(II) [30], Ni(II) [30], and Cu(II) [31] using metal adatom probe, nanogravimetry and chronoamperometry. Gooding and co-workers [42] studied GSH bonded to mercaptopropionic acid as the sensor for Cd(II). The interactions of adsorbed GSH with Cu^{2+} have also been studied [31,32]. It has been shown that GSH-SAM's formed

* Corresponding author. Fax: +1 315 267 3170.
E-mail address: hepelmr@potsdam.edu (M. Hepel).

0021-9797/$ - see front matter © 2010 Elsevier Inc. All rights reserved.
doi:10.1016/j.jcis.2010.06.010

on Au piezoelectrodes can act as chemically controlled ion gates [30,43–46] and as templates for metal depositions [31].

In living organism's homeostasis, GSH and its oxidized disulfide form (GSSG) constitute the main redox regulation system. It protects cells against organic peroxides and damaging radicals, and is involved in signaling processes associated with cell apoptosis. The diminished active GSH levels in cells and body fluids lead to the reduced antioxidation capacity [47] to protecting against radicals and have been found to increase susceptibility to autism [48,49], diabetes [50], and other diseases [47,49–55]. The low GSH levels have been found to be caused by oxidative stress and exposure to toxic heavy metals (Hg, Cd, Pb). GSH and phytochelatines with general structure $(\gamma\text{-Glu-Cys})_n$Gly participate as the capping agents [56,57] in heavy-metal sulfide nanoparticles formed in living organisms in natural detoxification processes [58–61].

The glutathione-mediated gold nanoparticle assembly has been studied by Sudeep et al. [36] and by Zhong and co-workers [37] and strong effects of pH and electrolyte concentration have been found. A model based on two-point zwitterionic interparticle interactions has been proposed [62]. Directional growth of GSH-linked gold nanorod assemblies has been observed by Kou et al. [63] whereas the competitive adsorption of GSH and thiolated oligonucleotides has been investigated by Ackerson et al. [64]. Recently, GSH has been found to participate in the degradation of Pt(II)-based DNA intercalators utilized in chemotherapy.

In this work, we have investigated interactions of glutathione with gold nanoparticles and explored the utility of the resonance elastic light scattering (RELS) spectroscopy to monitor GSH-induced AuNP assembly. This technique has been developed [65–70] as a sensitive technique for the detection of bioorganic complexes. The resonance elastic light scattering from molecules and nanoparticles in solution results from the absorption of photons followed by an immediate coherent re-emission of light in all directions without any energy loss [70]. We have recently applied RELS to study nanoparticle assembly [71] and found it to be very sensitive to supramolecular ensemble formation in the system homocysteine-citrate-fluorosurfactant-AuNP. In this paper, we describe new phenomena associated with the interactions of GSH with AuNP and elucidate the mechanism of the multi-step process leading to the assembly of GSH-capped AuNP networks. For the model system based on high concentration levels of GSH and short time-scale AuNP assembly, an unexpected non-Langmuirian ligand-exchange kinetics has been found. Details of the experiments and implications of this finding are discussed.

2. Materials and methods

2.1. Chemicals

All chemicals used for investigations were of analytical grade purity. L-glutathione reduced (GSH), minimum 99%, glutathione oxidized form (GSSG), tetrachloroauric(III) acid trihydrate ($HAuCl_4 \cdot 3H_2O$), 99.9+% metals basis, were purchased from Sigma Aldrich Chemical Company (Atlanta, GA, USA) and used as received. Sodium citrate dihydrate was obtained from J.T. Baker Chemical Co. (Phillipsburg, NJ, USA). Sodium borohydride ($NaBH_4$) was obtained from Fisher Scientific Company. Solutions were prepared using Millipore (Billerica, MA, USA) Milli-Q deionized water (conductivity σ = 55 nS/cm). They were deoxygenated by bubbling with purified argon.

2.2. Apparatus

The imaging analyses of Au nanoparticles were performed using high-resolution transmission electron microscopy (HR-TEM) with Model JEM-2010 (Jeol, West Chester, PA, USA) instrument (200 kV). The elastic light scattering spectra were recorded using LS55 Spectrometer (Perkin Elmer, Waltham, MA, USA) equipped with 20 kW Xenon light source operating in 8 μs pulsing mode allowing for the use of monochromatic radiation with wavelength from 200 nm to 800 nm with 1 nm resolution and sharp cut-off filters: 290, 350, 390, 430, 515 nm. The dual detector system consisted of a photomultiplier tube (PMT) and an avalanche photodiode. Pulse width at half height was less than 10 μs. The UV–Vis spectra were recorded using Perkin Elmer Lambda 50 Spectrophotometer in the range 220–1100 nm or Ocean Optics (Dunedin, FL, USA) Model R4000 Precision Spectrometer in the range from 340 nm to 900 nm.

2.3. Procedures

The Au nanoparticles were synthesized according to the published procedure [72]. Briefly, to obtain 5 nm AuNP, a solution of $HAuCl_4$ (10 mM, 2.56 mL) was mixed with a trisodium citrate solution (10 mM, 9.6 mL), ratio 1:3.75, and poured to distilled water (88 mL). The obtained solution was vigorously stirred and fresh cold $NaBH_4$ solution (5 mM, 8.9 mL) was added dropwise. Larger AuNP (22.5 nm dia.) were obtained by mixing 10 mL of $HAuCl_4$ (10 mM stock solution) with 4 mL of Na_3Cit (38.75 mM) and 86 mL of water. The obtained solution was vigorously stirred and fresh cold $NaBH_4$ solution (5 mM, 8.9 mL) was added dropwise. The solution slowly turned light gray and then ruby red. Stirring was maintained for 30 min. The obtained citrate-capped core–shell Au nanoparticles were stored at 4 °C. Their size was first estimated from UV–Vis surface plasmon absorption band shift and determined more precisely by HR-TEM imaging to be: 5.0 ± 0.9 nm (n = 85) and 22.5 ± 2.6 nm (n = 40); these nanoparticles are denoted as $AuNP_{5nm}$ and $AuNP_{22nm}$, respectively. No larger particle population was present. The concentrations of AuNP are given in moles of particles per 1 L of solution (usually, in the nM range). The size and distribution of AuNP were also tested using plasmonic absorbance spectra in UV–Vis. For instance, a clear surface plasmon band with λ_{max} = 516 nm for $AuNP_{5nm}$ and a low background beyond that wavelength indicate that no larger particles were present. This was also confirmed by TEM. The pH of AuNP solutions was maintained a citrate buffer (0.46 mM) at pH = 5 for storing and adjusted to 3.24 ± 0.03 before the experiments.

The glutathione stock solutions in water (10 mM) were protected from light and stored at 4 °C. The interactions of GSH with AuNP were monitored by UV–Vis absorption and resonant elastic light scattering (RELS).

Quantum mechanical calculations of electronic structure for Cit and GSH adsorbed on small gold-atom clusters Au_n were performed using modified Hartree–Fock methods [73,74] with 6-311G* basis set and pseudopotentials, semi-empirical PM3 method, and density functional theory (DFT) with B3LYP functional and 6-311G* basis set, embedded in Wavefunction Spartan 6 [74]. The electron density and local density of states (LDOS) are expressed in atomic units, au^{-3}, where 1 au = 0.529157 Å and 1 au^{-3} = 6.749108 $Å^{-3}$.

3. Results and discussion

3.1. Effect of GSH on resonance elastic light scattering of AuNP nanoparticles

Typical RELS spectrum for a citrate-capped $AuNP_{5nm}$ solution is presented in Fig. 1a, curve 1, for a constant excitation wavelength λ_{ex} = 640 nm (1.94 eV). The scattering intensity peak with a Gaussian peak shape centered at $\lambda_{em} = \lambda_{ex}$ = 640 nm and with a narrow linewidth of $\Delta\lambda$ = 14 nm confirms that the effects due to radiation broadening, density fluctuation, fluorescence, and inelastic Raman

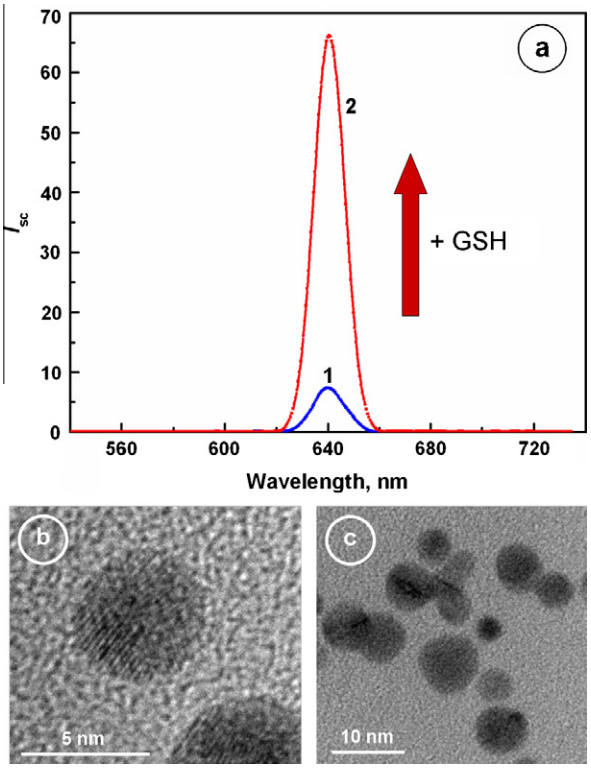

Fig. 1. Upper panel: (a) light scattering spectra for 10.1 nM $AuNP_{5nm}$ in the absence (1) and in the presence (2) of 5 mM glutathione, recorded for the incident beam wavelength λ_{ex} = 640 nm (spectra recorded within 1 min of glutathione injection). Lower panel: (b) high-resolution TEM image of $AuNP_{5nm}$; atomic rows with distance 0.24 nm are seen; (c) HR-TEM image of small GSH-linked $AuNP_{5nm}$ assemblies.

scattering are negligible. The background intensity is very low (virtually zero) providing excellent conditions for a sensitive analysis with well defined RELS peaks.

In the presence of GSH, the light scattering from $AuNP_{5nm}$ nanoparticles is strongly enhanced (Fig. 1a, curve 2). The solution pH was 3.24 ± 0.03 which is within the range of predominantly neutral (zwitterionic) form of GSH (pH = 2.04–3.4; pK_a values for GSH are: pK_1 = 2.04 (glutamate –COOH), pK_2 = 3.4 (glycine –COOH), pK_3 = 8.72 (–SH group), pK_4 = 9.49 ($-NH_2$ group)). Note that surface pK_a values may shift for surface-confined GSH similar to other molecules with pH-sensitive pendant groups ([75–81]), hence, these values are used only as guidelines. However, the strong RELS increase in pH range close to 3.2 confirms that zwitterionic form of GSH is in relative predominance in the AuNP shells, otherwise the assembly and strong scattering would not be observed. The enhancement of RELS from $AuNP_{5nm}$ by GSH molecules is attributed to the size increase of AuNP due to the ligand exchange (i.e. replacing short-chain citrate molecules in the nanoparticle shell with longer-chain GSH molecules) and/or interparticle interactions leading to AuNP assembly. The strong sixth-power dependence of elastic scattering intensity I_{sc} on the nanoparticle diameter a follows from the Rayleigh equation for light scattering from small particles:

$$I_{sc} = I_0 N \frac{(1+\cos^2\theta)}{2R^2}\left(\frac{2\pi}{\lambda}\right)^4 \frac{\left((n_p-n_s)^2-1\right)}{\left((n_p-n_s)^2+2\right)}\left(\frac{a}{2}\right)^6 \quad (1)$$

where n_p and n_s are the refractive indices for the particles and the solution, respectively, λ is the wavelength of incident light beam, θ is the scattering angle, N is the number of particles, and I_0 is the constant. Taking into account the decrease in particle concentration due to assembly and assuming λ = const and other experimental conditions (θ, R, I_0) unchanged, the increase of the effective particle diameter a_{rel} can be estimated using the formula [71]:

$$a_{rel} = \frac{a_1}{a_0} = \sqrt[3]{\frac{I_{sc,1}}{I_{sc,0}}} \quad (2)$$

where indices 0 and 1 stand for the particles before and after GSH addition, respectively. From the data of Fig. 1a, the scattering intensity increase is: $I_{sc,1}/I_{sc,0}$ = 9.09 and, hence, a_{rel} = 2.09. This means that most likely small aggregates composed of only few nanoparticles (e.g. 2–6) are formed. Similar experiments performed with larger Au nanoparticles show a completely opposite effect of GSH addition. In Fig. 2a, the RELS spectrum for a solution of $AuNP_{22nm}$ (C_{AuNP} = 1.42 nM) is shown in the absence of GSH (curve 1) and in the presence of 5 mM GSH (curve 2). Now, the addition of GSH to the Au nanoparticles, unexpectedly, results in a strong quenching of the Rayleigh scattering. To elucidate these differences in the behavior of $AuNP_{5nm}$ and $AuNP_{22nm}$, further investigations of full-scan RELS spectroscopy, long-term scattering evolution, and UV–Vis plasmonic spectroscopy have been carried out.

The full-scan RELS spectra for small and large AuNP are presented in Fig. 3. For small $AuNP_{5nm}$ nanoparticles, a dramatic increase of the resonant scattering intensity in the entire photon energy range scanned is observed. The I_{sc} maximum for $AuNP_{5nm}$ alone is at λ_{max} = 625 nm. The broad RELS peak generated by the interactions of GSH with $AuNP_{5nnm}$ is shifted to longer wavelengths and appears at λ_{max} = 655 nm. Similar RELS spectra forlarger nanoparticles ($AuNP_{22nm}$), presented in Fig. 3b, show that the I_{sc} maximum for $AuNP_{22nm}$ alone is larger than that for $AuNP_{5nm}$ alone, consistent with stronger scattering for larger particles. How-

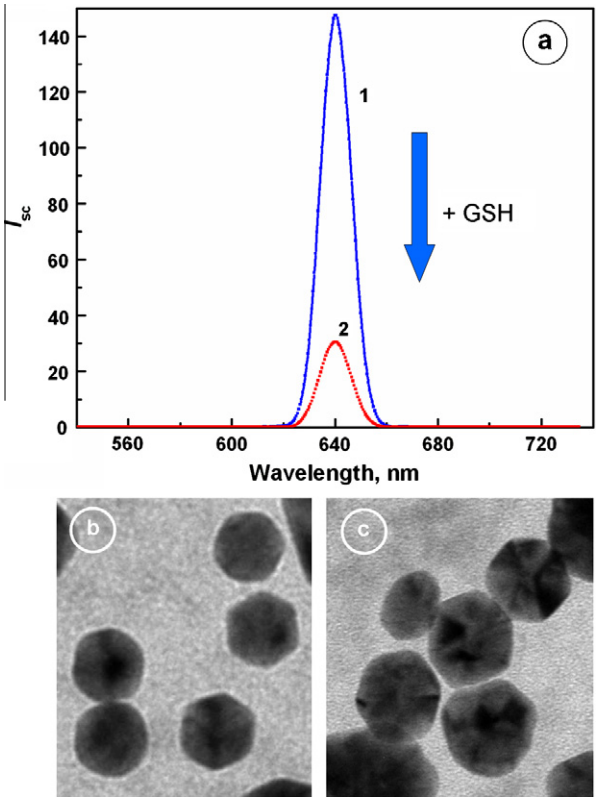

Fig. 2. Upper panel: (a) light scattering spectra for 1.42 nM $AuNP_{22nm}$, in the absence (1) and in the presence (2) of 5 mM glutathione (spectra recorded within 1 min of glutathione injection); incident beam wavelength: λ_{ex} = 640 nm. Lower panel: HR-TEM images of $AuNP_{22nm}$ before (b) and after (c) addition of 5 mM GSH.

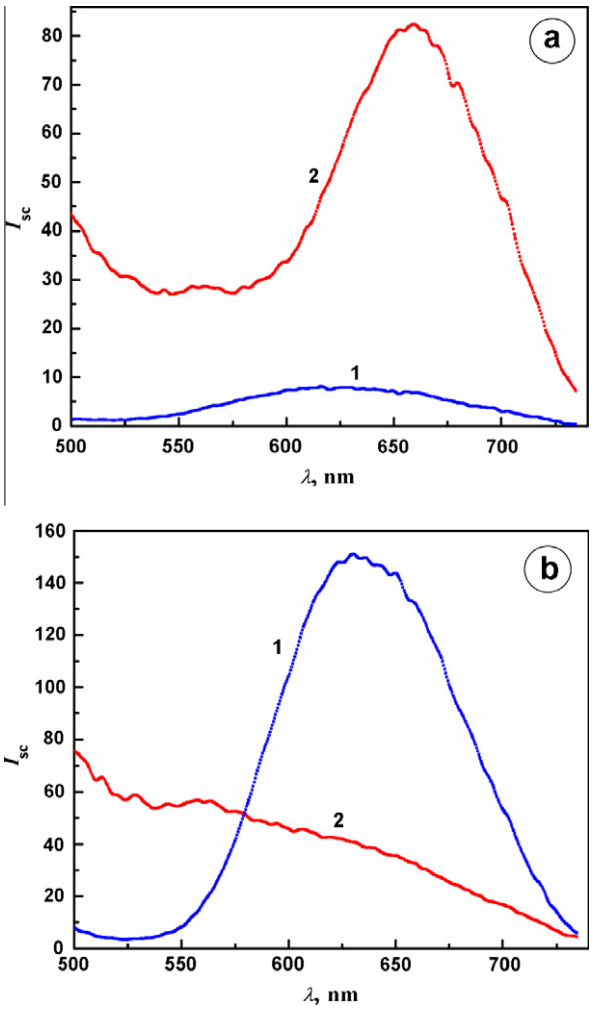

Fig. 3. RELS spectra I_{sc} vs. λ for: (a) small nanoparticles ($AuNP_{5nm}$) and (b) larger nanoparticles ($AuNP_{22nm}$) in the absence of GSH (1) and in the presence of 5 mM GSH (2), recorded within 1 min of GSH injection.

ever, in the presence of GSH an increase in scattering is only observed in the shorter wavelength region, $\lambda < 580$ nm, whereas a decrease in scattering intensity is apparent in the wavelength range above $\lambda = 580$ nm. The origin of the broad scattering peaks with $\lambda_{max} > \lambda_{SP,max}$ nm is ascribed to the increasing reflectivity of free electrons in Au at wavelengths longer than the Frohlich wavelength: $\lambda > \lambda_{Froh} = \lambda_{SP,max}$ where the electrical conductance of nanoparticles becomes a true metallic conductance [82]. At shorter wavelengths, the free conduction electrons in Au are unable to follow fast changing electromagnetic field imposed by the incident light beam.

The scattering intensity increases with nanoparticle concentration as illustrated in Fig. 4 where the dependencies of I_{sc} on C_{AuNP} for $AuNP_{5nm}$ and $AuNP_{22nm}$ are presented. A higher slope $\partial I_{sc}/\partial C_{AuNP}$ is encountered for $AuNP_{22nm}$ than for $AuNP_{5nm}$ consistent with the enhanced scattering by larger particles.

The relationship between the RELS intensity and GSH concentration for small Au nanoparticles, $AuNP_{5nm}$, measured after $\tau = 60$ s of reaction time does not conform to the Langmuirian pseudo-first-order kinetics. This is illustrated in RELS spectra presented in Fig. 5. The dependence of $I_{sc,max}$ on C_{GSH} is sigmoidal, as shown in Fig. 5b, curve 1, indicating on a kinetic threshold. This dependence indicates on the 2D nucleation and growth mechanism of the ligand-exchange process rather than uniform place-exchange mechanism, for which

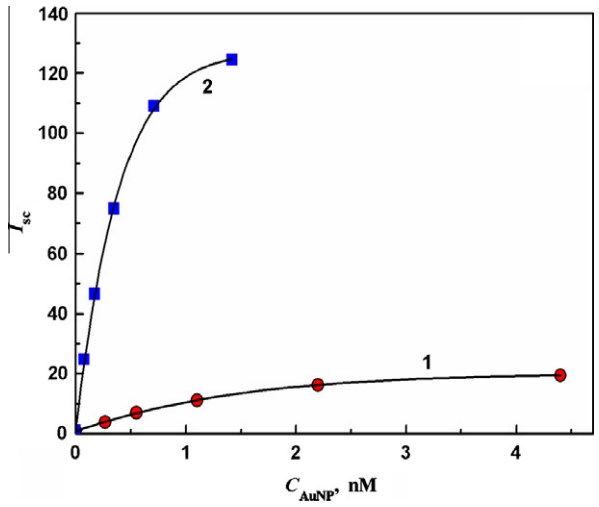

Fig. 4. Resonance elastic light scattering intensity I_{sc} on concentration of gold nanoparticles C_{AuNP} for: (1) $AuNP_{5nm}$ and (2) $AuNP_{22nm}$; incident beam wavelength: $\lambda_{ex} = 640$ nm.

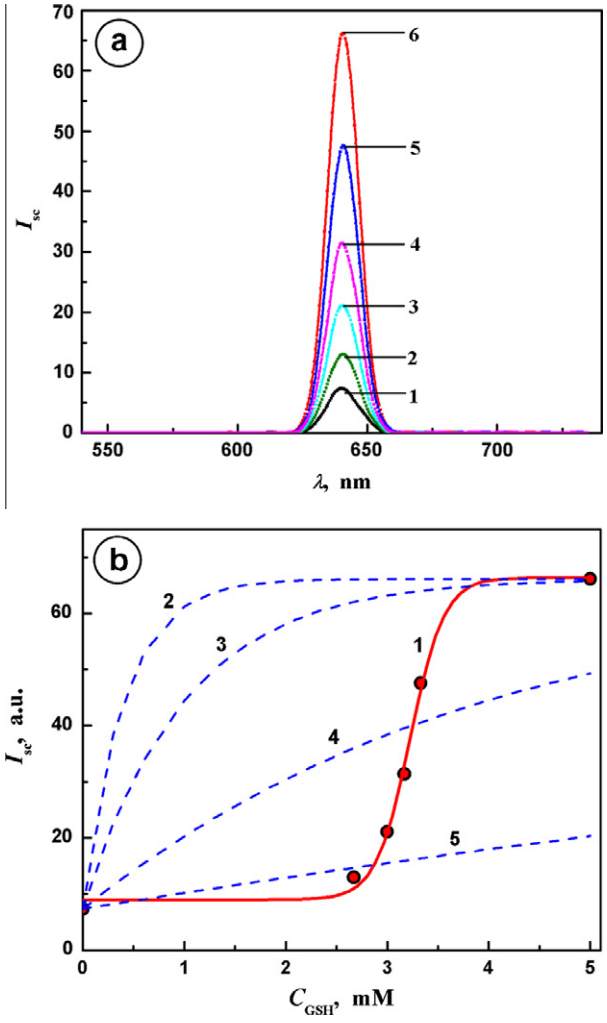

Fig. 5. (a) Elastic light scattering spectra for 10.1 nM $AuNP_{5nm}$ for different concentrations of GSH, recorded within 1 min of GSH injection, C_{GSH} [mM]: (1) 0, (2) 2.67, (3) 3.0, (4) 3.17, (5) 3.33, (6) 5; (b) experimental dependence of I_{sc} vs. C_{GSH} (curve 1, points) fitted with Boltzmann threshold function (line) and (2–5): calculated curves for a hypothetical pseudo-first-order Langmuirian kinetics showing the absence of threshold characteristics in Langmuirian model, k [$M^{-1}s^{-1}$]: (2) 40, (3) 17, (4) 4, (5) 0.8; $\tau = 60$ s; incident beam wavelength: $\lambda_{ex} = 640$ nm.

a pseudo-first-order Langmuirian kinetics describes well the ligand exchange and AuNP assembly in other systems [83–85]. To delineate the difference in the shape of the Langmuirian kinetic characteristics and the one observed experimentally, a family of kinetic curves was calculated for the rate constant values $k = 40$, 17, 4, and 0.8 $M^{-1}s^{1}$ (curves 2–5) using the kinetic equation [86] derived for random place-exchange assembly with pseudo-first-order Langmuirian kinetics:

$$I_{sc} = \varepsilon(1 - \exp\{-kC_{GSH}\tau\}) + I_{sc,ini} \quad (3)$$

where $\varepsilon = I_{sc,fin} - I_{sc,ini}$, k is the rate constant, τ is the reaction time, and $I_{sc,ini}$, $I_{sc,fin}$ are the RELS intensities at $\tau = 0$ and $\tau = \infty$, respectively. These curves show clearly the absence of any threshold in contrast to the experimental curves.

3.2. Evolution of surface plasmon absorbance of AuNP on interactions with GSH molecules

To corroborate the conclusion from previous section that gold nanoparticle assembly is responsible for the large scattering increase of $AuNP_{5nm}$ particles upon injection of GSH, we have performed measurements of the surface plasmon band shift under the same conditions as those for Fig. 1. A bathochromic SP band shift and a band broadening are indicative of the SP coupling occurring during the AuNP assembly process [36,37] and can thus be utilized to confirm the assembly. This type of UV–Vis spectroscopic evidence has been supported by the dynamic light scattering (DLS) measurements [33], small-angle X-ray scattering (SAXS) [33,87], and theoretical calculations of spectral shifts [1–5].

The color changes associated with ligand-exchange GSH-induced AuNP assembly are illustrated in Fig. 6. The concentration dependence of the SP absorbance band maximum $\lambda_{max} = f(C_{GSH})$ and $A_{max} = f(C_{GSH})$ recorded within 1 min of the reaction time do not represent a uniform ligand exchange, with GSH replacing the existing citrate SAM, but rather a 2D nucleation and growth process. It is seen that the threshold GSH concentration range is from 1.5 to 2.5 mM (Fig. 6b). The value of λ_{max} increases from $\lambda_{max,ini} = 522$ nm to the final value $\lambda_{max,fin} = 576$ nm at the plateau established for $C_{GSH} \geqslant 2.6$ mM. At the same time, A_{max} goes through a maximum and decreases at higher GSH concentrations. In the first stage, for $C_{GSH} < 2.28$ mM, absorbance maximum increases with C_{GSH} on account of the increasing diameter of GSH-capped AuNP ensembles, while in the second stage, for $C_{GSH} > 2.28$ mM, absorbance maximum decreases with further increase of C_{GSH} due to the bathochromic shift of the SP band to longer wavelength and natural $1/\lambda$ absorbance decrease. Note that the concentrations required to drive ligand exchange in 60 s of reaction time are much higher than those observed for small thiol molecules such as cysteine or homocysteine which are typically in the low micromolar range. Extensive studies of SP absorbance for various AuNP systems have been carried out by the Zhong group [33–35,88]. In particular, from studies of the GSH-mediated assembly of AuNP [37,62] it follows that the presence of NaCl (10 mM) stimulates GSH-mediated assembly of $AuNP_{11nm}$ while the addition of NaOH (1.6–3.3 mM) reverses it. In our experiments, the pH was maintained at pH = 3.24 ± 0.03 by citrate buffer which is within the range of zwitterionic predominance of GSH species.

The SP band broadening concomitant with bathochromic band shift is clearly observed in Fig. 6. The calculations of the SP band structure for gold and silver nanoparticles have been performed by various groups [1–6] enabling to assess the effects of the size and shape variability of nanoparticles, nanorods, and nanoplates, on plasmonic absorbance. The broadening of the SP band for AuNP has been described by El-Sayed et al. [2,3]. The SP band broadening and bathochromic band shift observed in our experiments corroborate the assembly process.

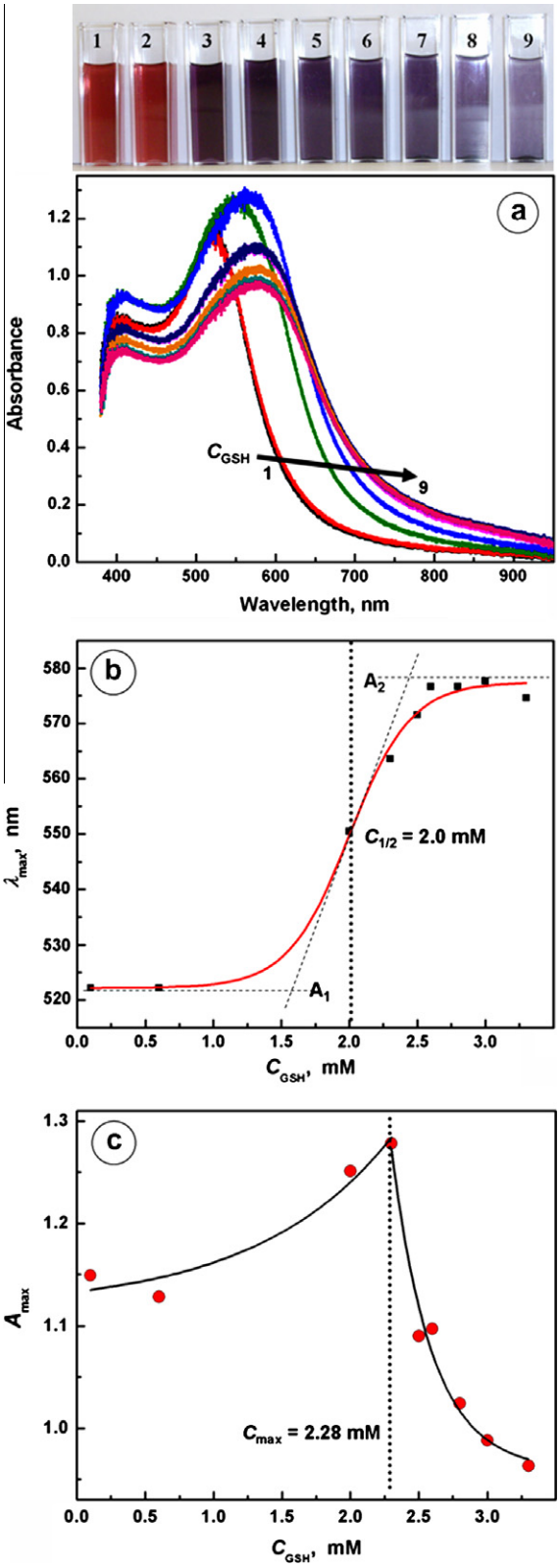

Fig. 6. Effect of glutathione concentration on absorbance of 10.1 nM $AuNP_{5nm}$ nanoparticle solution: (a) absorbance spectra for C_{GSH} [mM]: (1) 0.1, (2) 0.67, (3) 2.0, (4) 2.33, (5) 2.5, (6) 2.67, (7) 2.83, (8) 3.0, (9) 3.33; above: color change in response to GSH injections (1–9); (b) dependence of the surface plasmon band wavelength λ_{max} on C_{GSH}; (c) dependence of SP absorbance maximum A_{max} on C_{GSH}.

Similar experiments performed with oxidized glutathione GSSG (not shown) indicate that the transition concentration $C_{1/2,GSSG}$ for

half-way shift of peak wavelength λ_p is lower than that for the reduced GSH. For $AuNP_{5nm}$, $C_{1/2,GSSG}$ = 0.83 mM for GSSG for 1 min reaction time in comparison to $C_{1/2,GSH}$ = 2.0 mM for GSH, as determined from fitting of the Boltzmann function:

$$\lambda_p = \lambda_{p,\max} + \frac{(\lambda_{p,\min} - \lambda_{p,\max})}{\left(1 + \exp\left\{\frac{C - C_{1/2}}{s}\right\}\right)} \quad (4)$$

where $\lambda_{p,\min}$, $\lambda_{p,\max}$ – are the minimum and maximum values of the peak wavelength λ_p, $C_{1/2}$ is the concentration at the inflection point, and s is the slope parameter. The lower value of $C_{1/2}$ for GSSG than for GSH can be ascribed to the higher 2D nucleation rate for the disulfide where each GSSG molecule contributes 2 GS^- moieties to the forming 2D nucleus.

3.3. Long-term monitoring of GSH-mediated AuNP assembly by resonance light scattering

The temporal evolution of RELS signal at λ_{ex} = 640 nm, for a 2.5 nM $AuNP_{5nm}$, after addition of GSH (5 mM final concentration), is presented in Fig. 7, for the time span of 10 h. Immediately after GSH injection, a jump of scattering occurs (stage I). This initial reactivity, completed within 1 min of GSH injection, represents a straight vertical line in Fig. 7. As discussed in the next section, the ligand-exchange and GSH-mediated AuNP assembly into small ensembles are responsible for this large change in the scattering cross-section. The initial jump of scattering is followed by a slow exponential decrease of scattering (stages II and III) which is attributed to the film ordering and relaxation after the completion of the ligand-exchange and formation of small assemblies. This process lasts approximately 4.5 h. The duration of the first part of the decay (stage II) is approximately 1.5 h and results in a 12% decrease in RELS intensity. This period is then followed by ca. 3 h of very slow scattering changes (stage III of apparent colloid stability). After that a slow decay of scattering is observed (stage IV) which is due to C_{AuNP} depletion arising from the sedimentation of assemblies. Control experiments indicate on a decrease of absorbance and thus confirm the solution depletion due to sedimentation. This is also corroborated by the observation of precipitated networked AuNP material after 24 h. Larger particles (e.g. $AuNP_{22nm}$) are more likely to show screening of incident light for other $AuNP_{22nm}$ bound in ensembles. Also, the sedimentation begins immediately after the addition of GSH. These might be the main reasons why the decrease of RELS was observed in Fig. 2. To the increased speed of sedimentation may also contribute nanoparticle crystallinity which is higher for $AuNP_{22nm}$ than for $AuNP_{5nm}$ which are spherical. The $AuNP_{22nm}$ nanocrystals have large flat surfaces and the attachment of two particles becomes then much stronger since the interparticle interactions are stronger. This in turn induces the formation of larger aggregates for which both the screening is more efficient and precipitation is faster.

3.4. Mechanistic aspects of the interactions of GSH with AuNP

On the basis of measurements described in previous sections, we have evaluated the pathways of GSH interactions and reactivity with core–shell gold nanoparticles. Before presenting the mechanism, it is necessary to assess changes in the thickness of AuNP protecting monolayers. The thickness of a citrate shell around a AuNP is from 0.38 nm (flat orientation) to 0.70 nm (vertical, fully extended orientation) and the height of a GSH molecule adsorbed on a Au is on the order of 1.18 nm based on EQCN measurements and quantum chemical evaluation [30] for GSH adsorbed on solid QC/Au piezoelectrodes. The structure and dimensions of Cit and GSH molecules are shown in Fig. 8. During the ligand exchange (AuNP@Cit + GSH = AuNP@GSH + Cit), the diameter of a single

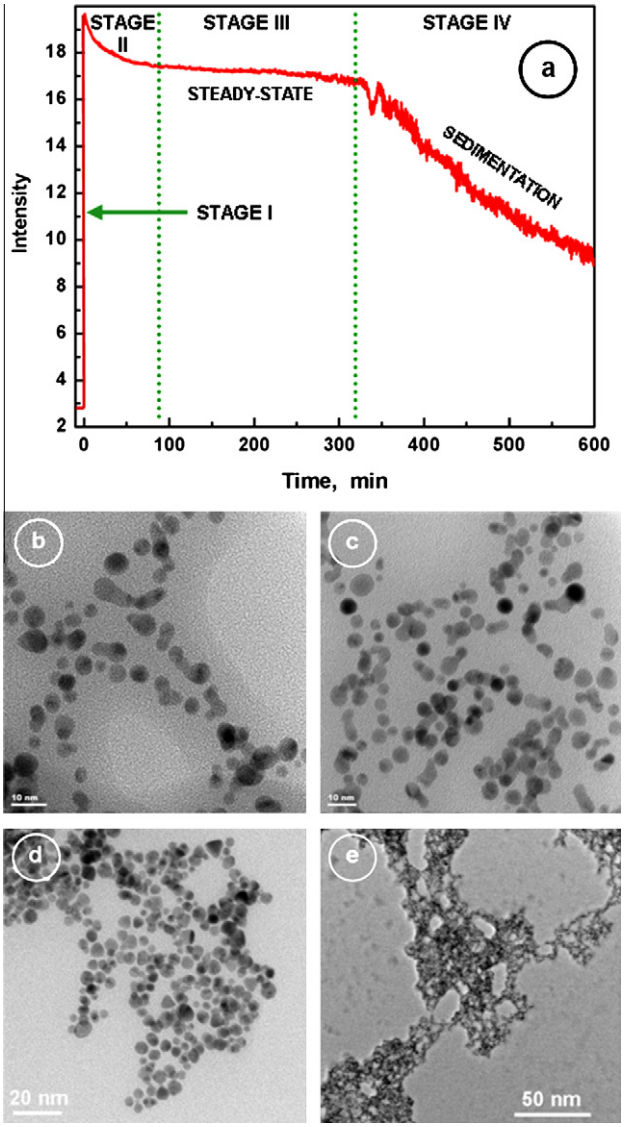

Fig. 7. Upper panel: (a) temporal evolution of RELS intensity at λ = 640 nm for a 2.5 nM $AuNP_{5nm}$ nanoparticle solution after injection of 5 mM GSH. Lower panel: HR-TEM images obtained during a GSH-induced AuNP assembly; increasing density of AuNP networks from (b) to (e).

AuNP, with core of 5 nm dia., would increase from ca. 6.4 nm to 7.4 nm, or by 15.6%. This is rather a small change of the diameter and so it cannot account for the observed 9-fold scattering intensity increase observed upon injection of GSH to $AuNP_{5nm}$ solution. The change in the refractive index on ligand replacement is small due to the similarity of organic shells and is thus neglected. Therefore, upon addition of GSH to a solution of citrate-capped AuNP, a GSH-mediated assembly of AuNP@GSH must take place.

According to our estimates based on RELS measurements, the diameter of the assemblies is approximately doubled (the effective diameter: a_1 = 2.1 a_0, where a_0 is the diameter of the original citrate-capped AuNP). The GSH-capped AuNP assemblies are depicted in Fig. 8.

During the film relaxation period (stage II), the newly formed GSH SAM is being compacted and the film ordering processes take place. It is also rational to assume that any intermediate structures composed of linker molecules present in the interparticle space are disassembled and removed in favor of more stable direct particle-to-particle bonding through the zwitterionic and H-bond forces.

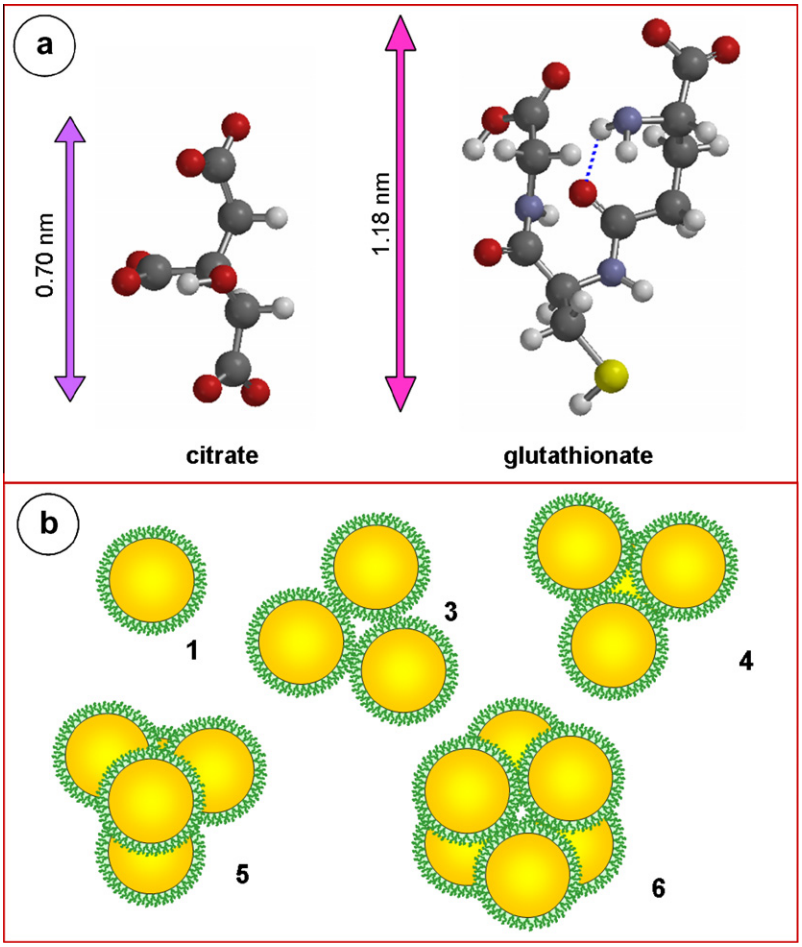

Fig. 8. (a) Comparison of heights of AuNP capping molecules: citrate and glutathionate (atoms: yellow – sulfur, red – oxygen, blue – nitrogen, gray – carbon, light gray – hydrogen); (b) small assemblies of n GSH-linked AuNP with diameter $2a_0 < a < 3a_0$ (n = 3 to 6, marked at the assemblies), where a_0 is the diameter of single AuNP (n = 1). (For interpretation of the references to color in this figure legend, the reader is referred to the web version of this article.)

3.5. Interparticle hydrogen bonding and electrostatic interactions

In order to verify the feasibility of the mechanism presented above, molecular dynamics simulations and quantum mechanical calculations of structural interdependencies of interacting molecular capping agents and cross-linkers were conducted.

The initiating interactions of GSH molecules with citrate-capped AuNP is likely to break hydrogen bonds between citrate molecules in the citrate SAM on AuNP making the citrate ligands more vulnerable to be pulled out the SAM. One example of such bonding between GSH linker and citrate-capped AuNP is presented in Fig. 9a. The ligand-exchange that follows leads to the complete replacement of weakly bound citrate SAM with more strongly bound GSH-SAM on account of the strong Au–S bonding. While in the stage I of GSH interactions with AuNP the ligand-exchange is completed, provided that sufficiently high concentration of GSH is used ($C_{GSH} > 2.5$ mM), it is likely that interparticle linker structures are formed which facilitate the fast assembly of AuNP, as indicated by the large jump in the scattering intensity. It is rational to assume that these structures (e.g. AuNP@GSH – GSH(aq) – AuNP@GSH) release the linker molecules during the relaxation stage II in favor of directly bonded particle-to-particle ensembles with strong zwitterionic and hydrogen bonding. An example of such interparticle bonding is presented in Fig. 9c. This process represents compacting of ensembles and is therefore reflected in the decrease of scattering. The experimental decrease of ca. 12% of scattering is consistent with this model. Due to the flexibility and intrinsic multiple-functionality of GSH ligands, a wealth of interparticle interactions becomes possible. Hence, the interparticle interactions of GSH-capped AuNP have been further analyzed by considering the formation of multiple hydrogen bonds as depicted in Fig. 10. It is seen that there are several possibilities for the formation of hydrogen bonds, from a single H-bond up to a triple H-bond. In Fig. 10a, a single H-bond COOH′–COOH″ formed between COOH groups from two GSH molecules is presented. In Fig. 10b, another single H-bond COOH–NH_2 is shown which forms between COOH group from one GSH molecule and NH_2 group from another GSH molecule. Then, in Fig. 10c–e, double H-bonds are presented. They can be formed as follows: (c) two H-bonds on the same couple COOH′–COOH″ where one carboxyl is from one GSH molecule and one from the second GSH molecule; (d) COOH′–COOH″ and COOH′–COOH‴, where the same COOH′ from one GSH molecule forms two H-bonds with two different carboxyl groups COOH″ and COOH‴ from the second GSH molecule; (e) one H-bond COOH′–NH_2 and one COOH″–COOH where two different carboxyl groups (COOH′ and COOH″) in one GSH molecule are involved. A triple H-bond is shown in Fig. 10f: two H-bonds in one carboxylate couple COOH′–COOH″ plus one H-bond COOH‴–NH_2. This means that there is a lot of configurational flexibility in GSH molecules to achieve one- to triple-H-bonding and thus the ensembles of GSH-capped AuNP are considerably strengthened by the selection of H-bonding opportunities.

The formation of hydrogen bonds is augmenting strong zwitterionic interactions due to the polarized groups COO^-–NH_3^+ operat-

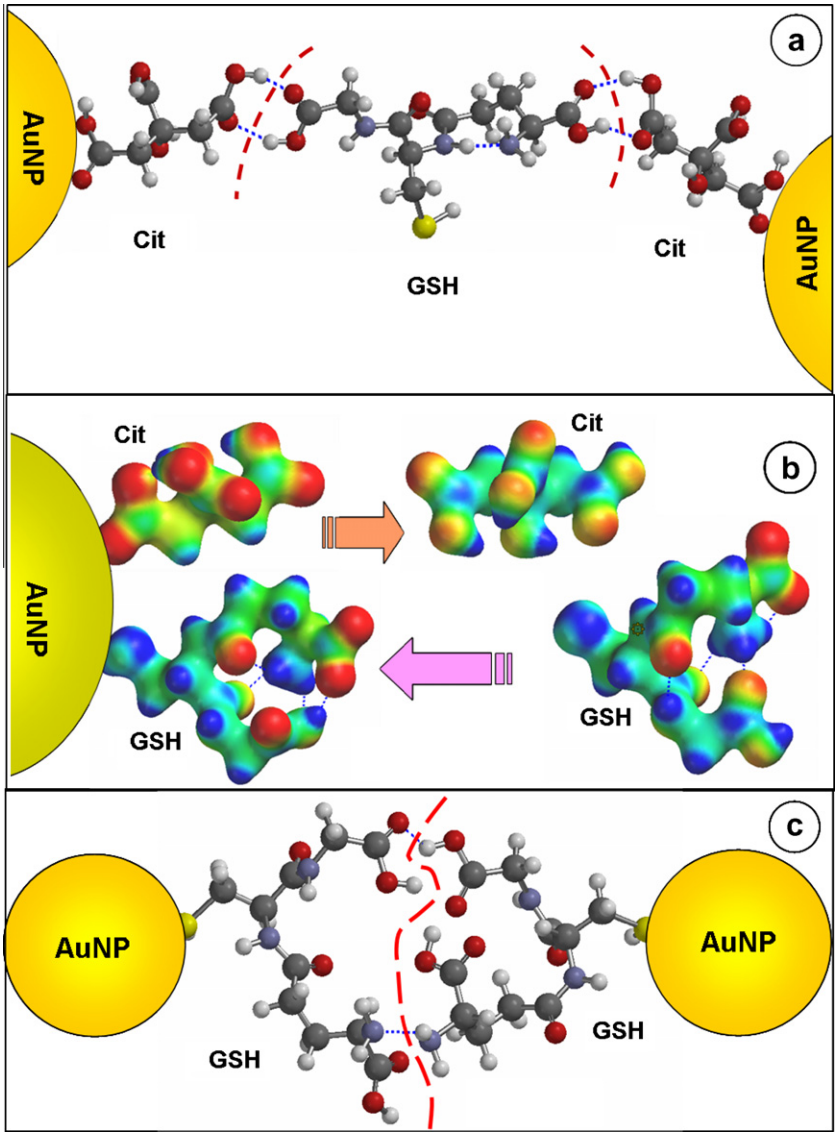

Fig. 9. Mechanism of interactions of GSH with gold nanoparticles: (a) formation of interparticle linkages, (b) ligand exchange, (c) interparticle hydrogen bonding; gold nanoparticles drawn not-to-scale; in (b): electron density surfaces for a model citric acid and glutathione for electron density $d = 0.1$ au^{-3}, color coded electrostatic potential: from blue – positive, to red – negative potential. Internal hydrogen bonds are also seen in citric acid and glutathione in (b). (For interpretation of the references to color in this figure legend, the reader is referred to the web version of this article.)

ing in the pH range from 2.04 to 3.4. At pH < 2.04 and pH > 3.4, electrostatic repulsions become the dominant force in the interparticle interactions between GSH-capped gold nanoparticles.

The results presented above corroborate the mechanism of interactions of glutathione molecules with citrate-capped gold nanoparticles, the formation of GSH linkages, and the interparticle interactions of AuNP.

4. Conclusions

We have demonstrated that RELS spectroscopy can provide a wealth of information about the interactions of small biomolecules, such as glutathione, with gold nanoparticles and can be applied to monitor the ligand-exchange processes followed by AuNP assembly. The RELS spectroscopic measurements, in conjunction with plasmonic UV–Vis absorbance and HR-TEM imaging, have revealed that the interactions of glutathione with gold nanoparticles are complex and proceed through several stages: (i) ligand-exchange and interparticle cross-linking resulting in AuNP assembly, (ii) relaxation of AuNP ensembles with GSH-SAM ordering and disassembly of interparticle linker structures evidenced by the decrease in light scattering, (iii) period of a metastable colloidal solution (steady-state), (iv) further aggregation with sedimentation. Strong dependence of scattering cross-section on GSH concentration has been found for small AuNP (5 nm dia.) with 9-fold increase of RELS intensity I_{sc} (for $C_{AuNP,5nm} \approx 10$ nM and $C_{GSH} > 2.5$ mM). The calculated effective diameter of assemblies is $2.1a_0$ indicating on the formation of small ensembles (2–6 original nanoparticles). For larger AuNP (22.5 nm dia.), an opposite effect has been observed where the addition of GSH caused a sharp decrease in I_{sc}, ascribed to more extensive assembly and sedimentation of aggregates. Indeed, the time-resolved assembly and sedimentation stages in GSH-linked AuNP network formation have been observed in long-term monitoring of GSH–AuNP interactions by RELS for smaller, more stable, $AuNP_{5nm}$ nanoparticle systems. The ligand exchange (citrate for GSH) has been found to deviate from the first-order Langmuirian kinetics observed for some longer chain thiols [83,84] and the obtained characteristics $I_{sc} = f(C_{GSH})$ appear to be a sigmoidal threshold

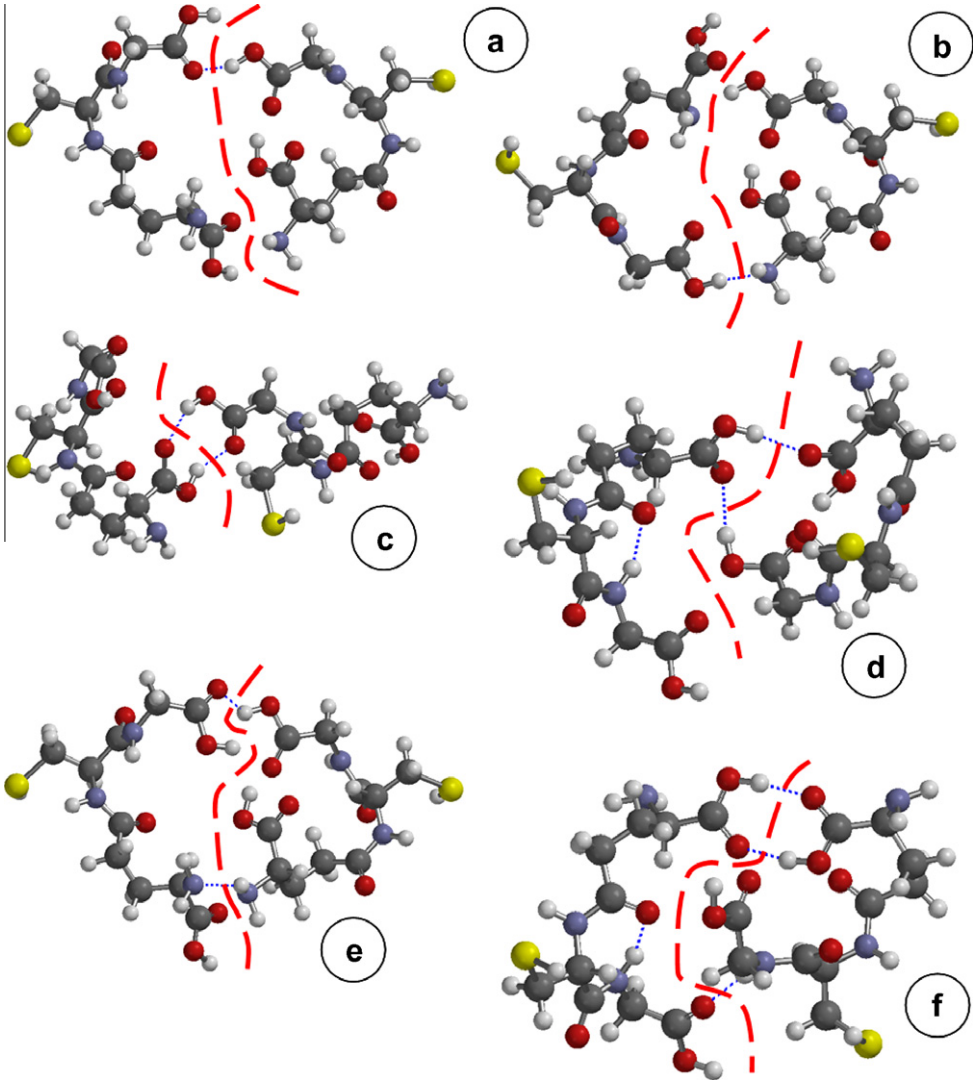

Fig. 10. Hydrogen bonding between two glutathione molecules from shells of two interacting AuNP; H-bonds marked with a dotted line; atoms: yellow – sulfur, red – oxygen, blue – nitrogen, gray – carbon, light gray – hydrogen); GSH molecules are separated with a red dashed line. (For interpretation of the references to color in this figure legend, the reader is referred to the web version of this article.)

function resembling that obtained recently for homocysteine ligand [71]. Such a ligand-exchange process is likely to encompass a 2D nucleation and growth process rather than a random place-exchange. The observed SP band broadening and bathochromic shift are consistent with the ligand-exchange and GSH-induced AuNP assembly. These control experiments support the conclusions drawn from the results of RELS measurements. Molecular dynamics and quantum mechanical calculations corroborate the interparticle interactions with zwitterionic and multiple H-bonding leading to GSH-induced AuNP assembly observed experimentally. We have found the RELS spectroscopy to be very useful in elucidating mechanistic aspects of interparticle interactions. The application of RELS can be expanded to monitor reactivities and assembly of other monolayer-protected metal clusters, especially for very fast processes which cannot be followed by other techniques.

Acknowledgments

This work was supported by the US DoD Research Program, Grant No. AS-073218. The help of students Zachary Reed and Justine Barcomb is acknowledged.

References

[1] K.L. Kelly, E. Coronado, L.L. Zhao, G.C. Schatz, J. Phys. Chem. B 107 (2003) 668–677.
[2] S. Link, M.A. El-Sayed, J. Phys. Chem. B 103 (1999) 8410–8426.
[3] S. Link, M.B. Mohamed, M.A. El-Sayed, J. Phys. Chem. B 103 (1999) 3073–3077.
[4] S. Franzen, J.C.W. Folmer, W.R. Glomm, R. O'Neal, J. Phys. Chem. B 106 (2002) 6533–6540.
[5] C. Ungureanu, R.G. Rayavarapu, S. Manohar, T.G.V. Leeuwen, J. Appl. Phys. 105 (2009) 102032.
[6] A.L. Gonzales, C. Noguez, J. Comput. Theor. Nanosci. 4 (2007) 231.
[7] M. Sugawara, A. Hirano, P. Buhlmann, Y. Umezawa, Bull. Chem. Soc. Jpn. 75 (2002) 187.
[8] J.J. Gooding, I. Pugliano, D.B. Hibbert, P. Erokhin, Electrochem. Commun. 2 (2000) 217.
[9] W.U. Wang, C. Chen, K.H. Lin, Y. Fang, Proc. Natl. Acad. Sci. U. S. A. 102 (2005) 3208–3212.
[10] M. Hepel, J. Dallas, M.D. Noble, Sensors Transducers J. 88 (2008) 47.
[11] M. Hepel, J. Dallas, M.D. Noble, J. Electroanal. Chem. 622 (2008) 173–183.
[12] I. Szymanska, M. Stobiecka, C. Orlewska, T. Rohand, D. Janssen, W. Dehaen, H. Radecka, Langmuir 24 (2008) 11239–11245.
[13] J. Halamek, M. Hepel, P. Skladal, Biosens. Bioelectron. 16 (2001) 253.
[14] J. Pribyl, M. Hepel, J. Halamek, P. Skladal, Sens. Actuators B 91 (2003) 333.
[15] J. Pribyl, M. Hepel, P. Skladal, Sens. Actuators B 113 (2006) 900.
[16] M. Stobiecka, J.M. Cieśla, B. Janowska, B. Tudek, H. Radecka, Sensors 7 (2007) 1462–1479.
[17] A.P. Alivisatos, K.P. Johnsson, X. Peng, T.E. Wilson, C.J. Loweth, M.P. Bruchez, P.G. Schultz, Nature 382 (1996) 610.
[18] S.J. Park, T.A. Taton, C.A. Mirkin, Science 295 (2002) 1503–1505.

[19] J.J. Storhoff, R. Elghanian, R.C. Mucic, C.A. Mirkin, R.L. Letsinger, J. Am. Chem. Soc. 120 (1998) 1959–1964.
[20] T.A. Taton, G. Lu, C.A. Mirkin, J. Am. Chem. Soc. 123 (2001) 5164–5165.
[21] T.A. Taton, R.C. Mucic, C.A. Mirkin, R.L. Letsinger, J. Am. Chem. Soc. 122 (2000) 6305–6306.
[22] R.A. Reyolds, C.A. Mirkin, R.L. Letsinger, J. Am. Chem. Soc. 122 (2000) 3795–3796.
[23] I.I.S. Lim, U. Chandrachud, L. Wang, S. Gal, C.J. Zhong, Anal. Chem. 80 (2008) 6038–6044.
[24] R. Elghanian, J.J. Storhoff, R.C. Mucic, R.L. Letsinger, C.A. Mirkin, Science 277 (1997) 1078–1081.
[25] B. Dubertet, M. Calame, A.J. Libchaber, Nat. Biotechnol. 19 (2001) 365–370.
[26] E. Matijevic, Medical Applications of Colloids, Springer Sci., New York, 2008.
[27] L. Tong, Y. Zhao, T.B. Huff, M.N. Hansen, A. Wei, J.X. Cheng, Adv. Mater. (Weinheim, Germany) 19 (2007) 3136.
[28] T.B. Huff, L. Tong, Y. Zhao, M.N. Hansen, J.X. Cheng, A. Wei, Nanomedicine 2 (2007) 125.
[29] C.H. Chou, D. Chen, C.R.C. Wang, J. Phys. Chem. B 109 (2005) 11135.
[30] M. Hepel, E. Tewksbury, J. Electroanal. Chem. 552 (2003) 291–305.
[31] M. Hepel, E. Tewksbury, Electrochim. Acta 49 (2004) 3827–3840.
[32] C. Fang, X. Zhou, Electroanalysis 15 (2002) 1632–1638.
[33] M.M. Maye, I.I.S. Lim, J. Luo, Z. Rab, D. Rabinovich, T. Liu, C.J. Zhong, J. Am. Chem. Soc. 127 (2005) 1519–1529.
[34] I.I.S. Lim, W. Ip, E. Crew, P.N. Njoki, D. Mott, C.J. Zhong, Langmuir 23 (2007) 826–833.
[35] F.X. Zhang, L. Han, L.B. Israel, J.G. Daras, M.M. Maye, N.K. Ly, C.J. Zhong, Analyst 127 (2002) 462–465.
[36] P.K. Sudeep, S.T.S. Joseph, K.G. Thomas, J. Am. Chem. Soc. 127 (2005) 6516–6517.
[37] I.M.S. Lim, D. Mott, W. Ip, P.N. Njoki, Y. Pan, S. Zhou, C.J. Zhong, Langmuir 24 (2008) 8857–8863.
[38] Z.P. Li, X.R. Duan, C.H. Liu, B.A. Du, Anal. Biochem. 351 (2006) 18.
[39] S. Mandal, A. Gole, N. Lala, R. Gonnade, V. Ganvir, M. Sastry, Langmuir 17 (2001) 6262.
[40] P.R. Selvakannan, S. Mandal, S. Phadtare, R. Pasricha, M. Sastry, Langmuir 19 (2003) 3545.
[41] M. Hepel, J. Dallas, Sensors 8 (2008) 7224–7240.
[42] E. Chow, D.B. Hibbert, J.J. Gooding, Analyst 130 (2005) 831.
[43] K. Takehara, M. Aihara, Y. Miura, F. Tanaka, Bioelectrochem. Bioenerg. 39 (1996) 135.
[44] K. Takehara, M. Aihara, N. Ueda, Electroanalysis 6 (1994) 1083.
[45] K. Takehara, Y. Ide, M. Aihara, Bioelectrochem. Bioenerg. 29 (1991) 113.
[46] K. Takehara, Y. Ide, M. Aihara, E. Obuchi, Bioelectrochem. Bioenerg. 29 (1992) 103.
[47] M. Noble, M. Mayer-Proschel, C. Proschel, Antioxid. Redox Signaling 7 (2005) 1456–1467.
[48] S. Bernard, A. Enayati, L. Redwood, H. Roger, T. Binstock, Med. Hypotheses 56 (2001) 462–471.
[49] T. Clark-Taylor, Med. Hypotheses 62 (6) (2003) 970–975.
[50] K.M. Beard, N. Shangari, B. Wu, P.J. O'Brien, Mol. Cell. Biochem. 252 (2003) 331.
[51] G. Polidoro, C.D. Ilio, A. Arduini, G.L. Rovere, G. Federici, Int. J. Biochem. 16 (1984) 505–509.
[52] G. Almazzan, H.N. Liu, A. Knorchid, S. Sundararajan, A.K. Martinez-Bermudez, S. Chemtob, Free Radical Biol. Med. 29 (2000) 858–869.
[53] M. Repetto, C. Reides, M.L.G. Carretero, M. Costa, G. Griemberg, S. Llesuy, Clin. Chim. Acta 255 (1996) 107–117.
[54] S. Upadhya, S. Upadhya, S.K. Mohan, K. Vanajakshamma, M. Kunder, S. Mathias, Indian J. Clin. Biochem. 19 (2004) 80–83.
[55] T.W. Clarkson, Environ. Health Perspect. 100 (1992) 31–38.
[56] C.T. Dameron, R.N. Reese, R.K. Mehra, P.J. Kortan, M.L. Carrol, M.L. Steigerwald, L.E. Brus, D.R. Winge, Nature 338 (1989) 596.
[57] J. Barbas, V. Santhanagopalan, M. Blaszczynski, W.R. Ellis, D.R. Winge, J. Inorg. Biochem. 48 (1992) 95.
[58] O.K. Vatamaniuk, S. Mari, Y. Lu, P.A. Rea, J. Biol. Chem. 275 (2000) 31451–31459.
[59] O.K. Vatamaniuk, E.A. Bucher, J.T. Ward, P.A. Rea, J. Biol. Chem. 276 (2001) 20817.
[60] R.K. Mehra, D.R. Winge, J. Cell. Biochem. 45 (1991) 30.
[61] M. Inouhe, Braz. J. Plant Physiol. 17 (2005) 65–78.
[62] S. Zhang, X. Kou, Z. Yang, Q. Shi, G.D. Stucky, L. Sun, J. Wang, C. Yan, Chem. Commun. (2007) 1816.
[63] X. Kou, S. Zhang, Z. Yang, C.K. Tsung, G.D. Stucky, L. Sun, J. Wang, C. Yan, J. Am. Chem. Soc. 129 (2007) 6402.
[64] C.J. Ackerson, M.T. Sykes, R.D. Kornberg, Natl. Acad. Sci. U. S. A. 102 (2005) 13383.
[65] R.F. Pasternack, C. Bustamante, P.J. Collings, A. Giannetto, E.J. Gibbs, J. Am. Chem. Soc. 115 (1993) 5393–5399.
[66] R.F. Pasternack, Science 269 (5226) (1995) 935.
[67] Y.T. Wang, F.L. Zhao, K.A. Li, S.Y. Tong, Anal. Chim. Acta 396 (1999) 75–81.
[68] Z.X. Guo, H.X. Shen, Anal. Chim. Acta 408 (2000) 177–182.
[69] X. Wu, U.Y. Wang, M. Wang, S. Sun, J. Yang, Y. Luan, Spectrochim. Acta A 61 (2005) 361–366.
[70] Z. Jia, J. Yang, X. Wu, C. Sun, S. Liu, F. Wang, Z. Zhao, Spectrochim. Acta A 64 (2006) 555–559.
[71] M. Stobiecka, J. Deeb, M. Hepel, Biophys. Chem. 146 (2010) 98–107.
[72] J. Turkevich, P.C. Stevenson, J. Hiller, Discuss. Faraday Soc. 11 (1951) 55–75.
[73] P.W. Atkins, R.S. Friedman, Molecular Quantum Mechanics, Oxford University Press, Oxford, 2004.
[74] W.J. Hehre, L. Radon, P.R. Schleyer, J.A. Pople, Ab-initio Molecular Orbital Theory, Wiley, New York, 1985.
[75] A.C. Templeton, W.P. Wuelfing, R.W. Murray, Acc. Chem. Res. 33 (2000) 27–36.
[76] C.J. Zhong, M.D. Porter, J. Am. Chem. Soc. 116 (1994) 11616.
[77] J.F. Smalley, K. Chalfant, S.W. Feldberg, T.M. Nahir, E.F. Bowden, J. Phys. Chem. B 103 (10) (1999) 1676–1685.
[78] J. Luo, N. Kariuki, L. Han, M.M. Maye, L.W. Moussa, S.R. Kowaleski, F. Louis Kirk, M. Hepel, C.J. Zhong, J. Phys. Chem. B 106 (36) (2002) 9313–9321.
[79] M.A. Porter, J.R. Hall, J.C. Locke, J.H. Jensen, P.A. Molina, Proteins: Struct., Funct., Bioinf. 63 (3) (2006) 621–635.
[80] A.T. Masheter, P. Abiman, G.G. Wildgoose, E. Wong, L. Xiao, N.V. Rees, R. Taylor, G.A. Attard, R. Baron, A. Crossley, J.H. Jonesd, R.G. Compton, J. Mater. Chem. 17 (2007) 2616–2626.
[81] R.K. Shervedani, Electroanalysis 20 (5) (2008) 550–557.
[82] S. Franzen, J.C.W. Folmer, W.R. Glomm, R. O'Neal, J. Phys. Chem. A 106 (2002) 6533–6540.
[83] R. Georgiadis, K.P. Peterlinz, A.W. Peterson, J. Am. Chem. Soc. 122 (2000) 3166–3173.
[84] A. Kassam, G. Bremner, B. Clark, G. Ulibarri, R.B. Lennox, J. Am. Chem. Soc. 128 (2006) 3476–3477.
[85] I.I.S. Lim, M.M. Maye, J. Luo, C.J. Zhong, J. Phys. Chem. B 109 (2005) 2578–2583.
[86] M. Stobiecka, M. Hepel, Sens. Actuators, submitted for publication.
[87] A.E. Saunders, M.B. Sigman, B.A. Korgel, J. Phys. Chem. B 108 (2004) 193–199.
[88] I.I.S. Lim, F. Goroleski, D. Mott, N. Kariuki, W. Ip, J. Luo, C.J. Zhong, J. Phys. Chem. B 110 (2006) 6673–6682.